RSC Advances

PAPER

View Article Online
View Journal | View Issue

Cite this: *RSC Adv.*, 2022, **12**, 22197

Effect of water-soluble fullerenes on macrophage surface ultrastructure revealed by scanning ion conductance microscopy†

Hefei Ruan, ‡*[ab] Xuejie Zhang,‡[c] Jinghe Yuan[a] and Xiaohong Fang *[a]

Received 14th April 2022
Accepted 31st July 2022

DOI: 10.1039/d2ra02403a

rsc.li/rsc-advances

C_{60}-fullerenes have unique potential in antiviral, drug delivery, photodynamic therapy and other biomedical applications. However, little is known about their effects on macrophage surface morphology and ultrastructure. Here by using contact-free scanning ion conductance microscopy (SICM), we investigated the effects of two water-soluble fullerenes on the surface ultrastructure and function of macrophages. The results showed that these fullerenes would be a promising phagocytosis inhibitor and SICM would be an excellent tool to study the morphological information of adhesive and fragile samples.

Introduction

C_{60}-fullerene was discovered by Richard Smalley, Robert Curl and Harold Kroto in 1985 and it is a novel carbon allotrope with a spherical structure.[1,2] During the last few years, due to their unique physical structure and chemical properties,[3,4] C_{60}-fullerenes and their derivatives have been considered important ingredients for cosmetics and photoelectric materials, and they also have many advantages and potential in the field of biomedicine, such as antiviral, drug delivery and photodynamic therapy applications.[5–8] As an important molecule widely used in various biological activities, evaluating its cytotoxicity and biocompatibility to the immune system has become a very meaningful research topic in recent years.[9,10] Up to now, research on cytotoxicity and biocompatibility of some C_{60}-fullerenes mainly focused on detecting the release of inflammatory cytokines and cell viability in cultured macrophages.[11–13] For example, Park *et al.* found that carbon fullerenes (C_{60}s) could induce an increase in pro-inflammatory cytokines such as interleukin-1, tumor necrosis factor-α and interleukin-6 in the lung of mice.[14] Sayes *et al.* found that water-soluble nano-C_{60} colloidal suspension could disrupt normal cellular function through lipid peroxidation.[15] However, little is known about effects of C_{60}-fullerenes and its derivatives on the surface morphology and ultrastructural changes of macrophages. In addition, changes in cell morphology and surface ultrastructure are not only a reflection of the cytotoxicity and biocompatibility of nanomaterials, but also some cellular functions, *e.g.*, the phagocytosis of macrophage. For example, we can know whether the macrophage have an inflammatory reaction from its surface morphology,[16,17] and also it has been proved that cytoskeletal rearrangement and morphological changes can affect the phagocytic function of macrophages.[18,19]

The morphology of macrophages can be studied by using different imaging techniques, such as optical microscopy, atomic force microscopy (AFM), electron microscopy, *etc.* Due to the optical diffraction limit of traditional optical microscopy, the most common methods to study the surface ultrastructure of macrophage in nanoscale are AFM and electron microscopy. For example, AFM imaging was used to reveal the distinct features of macrophage ultrastructure for the different stages of phagocytosis against cancer cells.[20] Shvedova *et al.* studied the ultrastructural and morphological changes of human epidermal keratinocytes after treated with single-wall carbon nanotubes (SWCNTs) by scanning electron microscopy (SEM) and transmission electron microscopy (TEM),[21] Fiorito *et al.* revealed the changes of macrophage surface morphology after being treated with C_{60}-fullerenes and SWCNTs by SEM.[17] However, because of the contact scanning mode of AFM and extremely severe imaging conditions of electron microscopy, such as high vacuum conditions, electron beam excitation and freeze-dehydrated sample preparation, they all have potential damage to the surface ultrastructure of biological samples.[22] Therefore, a contact-free imaging technology with nanoscale resolution under physiological conditions is needed. Scanning ion conductance microscopy (SICM), an excellent combination of scanning probe microscopy (SPM) and patch-clamp technique, has been invented since 1989.[23] In the past few years, owing to the continuous improvements in the feedback control

[a]*Key Laboratory of Molecular Nanostructure and Nanotechnology, CAS Research/Education Center for Excellence in Molecular Sciences, Institute of Chemistry, Chinese Academy of Sciences, Beijing, China. E-mail: ruanhefei@iccas.ac.cn; xfang@iccas.ac.cn*

[b]*Tsinghua-Peking University Joint Center for Life Sciences, School of Medicine, Tsinghua University, Beijing, China*

[c]*Collaborative Innovation Center of Assessment Toward Basic Education Quality, Beijing Normal University, Beijing, China*

† Electronic supplementary information (ESI) available. See https://doi.org/10.1039/d2ra02403a

‡ These authors contributed equally to this work.

system, SICM has emerged as a powerful tool to image and analyze fragile, adhesive or sensitive surfaces, such as living cell membrane, with nanometer scale resolution.[24–27] For example, SICM can be used for long-term microvilli dynamics imaging with high image quality while AFM cannot.[28] Novak *et al.* tracked the dynamic interactions between individual carboxyl-modified nanoparticles and cell membrane structures at nanoscale using a high-speed SICM.[29] In addition, SICM also was used to evaluate the cytotoxicity and efficiency of many nanomaterials as drug delivery carriers by imaging the detailed cellular morphological information, *e.g.*, Lee *et al.* studied the morphological changes of A549 cells after treatment with doxorubicin-loaded DNA-wrapped halloysite nanotubes (HDD), they found that the actin filaments were disrupted into separated dot structures because of the release of doxorubicin from HDD.[30] Therefore, the contact-free SICM imaging technology provides an excellent method for studying the effects of fullerenes on the morphology and ultrastructure of macrophages under physiological conditions. In this work, we studied the surface ultrastructure of THP-1 macrophages before and after polyhydroxylated (C_{60}–OH) or cationic (C_{60}–Por) water-soluble fullerenes treatment by SICM under physiological conditions. Results indicate that the water-soluble fullerenes can affect the phagocytic function of macrophages by affecting their surface ultrastructure.

Results and discussion

Changes in macrophage surface ultrastructure such as membrane ruffles are closely related to macropinocytosis and phagocytosis, which in turn affect macrophage uptake and destruction of microbial pathogens. Therefore, it is important to use a non-contact and non-invasive method to characterize the adhesive and fragile ultrastructure on the surface of macrophages.[31] Here, for the first time, we imaged the surface ultrastructure of THP-1 differentiated macrophage using the contact-free SICM at nanoscale resolution under physiological conditions. Fig. 1A shows the schematic diagram of the SICM device with a nanopipette filled and immersed in physiological buffer above a biological sample. It is noted that THP-1 cells were incubated with PMA for 72 hours to induce differentiation and attachment before SICM imaging. By imaging the whole cell in a large scale, the cell surface exhibited many blurred structural details (Fig. 2A). Further small-scale imaging showed that there were many flat sheet-like membrane ruffles and a few circular ruffles on the dorsal membrane (Fig. 2B). As might be expected, almost all the membrane ruffles in SICM imaging appeared more intact while part of them seemed fractured in SEM imaging.[17,32] Therefore, studying the intact forms of these ruffles by contact-free SICM imaging might contribute to improving our understanding of phagocytosis and macropinocytosis mechanism.

In view of the great potential of C_{60}-fullerene derivatives in biomedical research, and the close relationship between macrophage surface morphology and cell function.[33,34] Therefore, investigating the effects of C_{60}-fullerene derivatives on the macrophage surface morphology and ultrastructure is of great

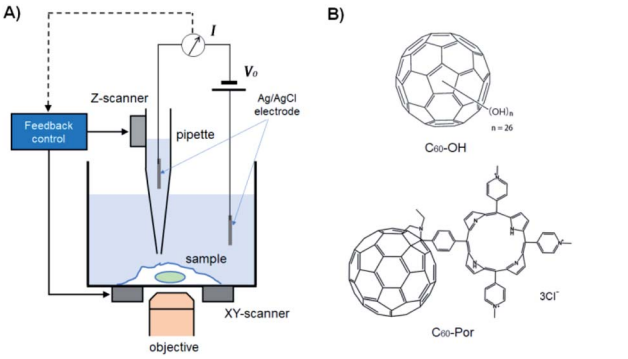

Fig. 1 (A) Schematic diagram of the SICM device with a nanopipette filled and immersed in physiological buffer above a biological sample. (B) Molecular structure of the hydroxyl and porphyrin-modified water-soluble fullerenes used in this study.

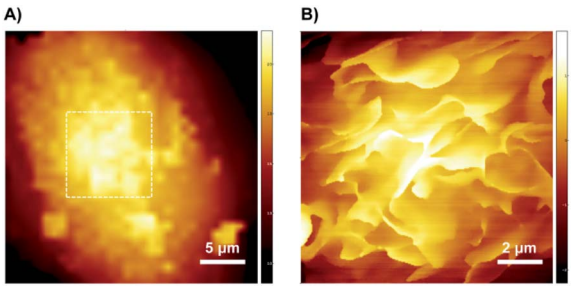

Fig. 2 SICM imaging of THP-1 differentiated macrophage surface ultrastructure. (A) The cell surface morphology of a large scale. (B) Further small-scale imaging showed the height topography on the dorsal membrane of macrophage. Region: 10 × 10 μm, pixel: 256 × 256.

significance. Here we observed the ultrastructure changes of THP-1 macrophage by SICM imaging after 48 hours of treatment with water-soluble fullerenes C_{60}–OH or C_{60}–Por (the molecular structures of the two are shown in Fig. 1B, and their hydration diameter was characterized by dynamic light scattering in ESI Fig. S1†). As shown in Fig. 3A and B, both the cells treated with 0.01 mg mL^{-1} C_{60}–OH or C_{60}–Por showed surface actin cytoskeleton rearrangement significantly (a higher concentration of 0.1 mg mL^{-1} was also studied in the ESI Fig. S2†). The sheet-like membrane ruffles become smaller and reduced after treated with C_{60}–OH, but more circular ruffles and blebs emerged. Contrary to these changes, the sheet-like ruffles become thickening and increased after C_{60}–Por treatment. In addition, we analyzed the length distribution of the membrane ruffles before and after water-soluble C_{60}-fullerenes treatment (Fig. 3C). The length of the membrane ruffles is about 7 μm before C_{60}-fullerenes treatment, but reduced to about 5 μm after C_{60}–Por treatment and about 2.5 μm after C_{60}–OH treatment. Taking these significant changes into account, we performed a cytotoxicity assay on the two water-soluble C_{60}-fullerenes. We evaluated the cytotoxicity of C_{60}–OH and C_{60}–Por against THP-1 macrophage by Cell Counting Kit-8 (CCK-8) assay. The result showed that more than 90% of the cells survived, so these two

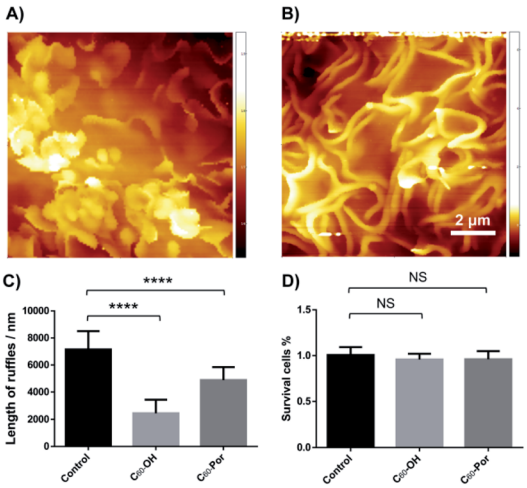

Fig. 3 The surface topography of THP-1 macrophages treated with different water-soluble C_{60}-fullerenes. (A) C_{60}–OH treatment. (B) C_{60}–Por treatment. (C) Length distribution of the surface membrane ruffles after different treatment. (D) Cytotoxicity of different C_{60}-fullerenes.

water-soluble C_{60}-fullerenes did not cause any statistically significant cytotoxicity (Fig. 3D). It is noted that the treatment concentrations and incubation times of water-soluble C_{60}-fullerenes in this study were based on the results of our previous study.[35,36] Therefore, the significant changes of surface membrane ruffles might be attributed to the activation of phagocytosis, rather than the cytotoxicity of C_{60}–OH and C_{60}–Por.

To study whether these surface actin cytoskeleton rearrangements were reversible or not, we removed the C_{60}-fullerenes and kept the THP-1 macrophages continuing to be cultured in normal medium for 48 hours. The SICM imaging showed that both the membrane ruffles could restore basically (Fig. 4). The surface membrane ruffles after treated with C_{60}–OH restored to large and sheet-like (Fig. 4A). As shown in Fig. 4B, the membrane ruffles of C_{60}–Por treated macrophages restored to sheet-like and showed a dramatic decrease.

Since the intracellular cytoskeleton plays an equally important role in the regulation of macropinocytosis and phagocytosis as well as surface ultrastructure, here we study whether the C_{60}–OH and C_{60}–Por fullerenes affect cell morphology through cytoskeletal fluorescence imaging. As shown in Fig. 5, the distribution of F-actin, stained by rhodamine phalloidin, was examined by a laser scanning confocal fluorescence microscope. Before treated with water-soluble C_{60}-fullerenes, PMA-differentiated THP-1 macrophages were adherent growth and they showed a spindle or polygonal morphology (Fig. 5A). The spindle or polygonal morphology could be mainly attributed to the important role of actin cytoskeleton. After C_{60}–OH or C_{60}–Por treatment, although both the cells were still adherent growth, most of them turned round (Fig. 5B and D). It heralded the rearrangement of the macrophage actin cytoskeleton. Then we removed the C_{60}-fullerenes and continued to culture the THP-1 macrophages in normal medium for 48 hours. Most of them restored to spindle or polygonal morphology and its surface ruffles have a certain degree of recovery (Fig. 5C and E). During this process, although we can see some changes in surface folds, these changes are not as pronounced compared to SICM imaging.

As mentioned above, the cellular morphology and surface ultrastructure of THP-1 macrophages changed significantly after water-soluble C_{60}–OH or C_{60}–Por treatment, and these changes were closely related to phagocytic function. Therefore, studying the changes of macrophage phagocytosis before and after C_{60}-fullerenes treatment is beneficial to understand the impact on its immune function. In our experiment, THP-1 macrophages were exposed to fluorescent beads with a diameter of 2 μm overnight after C_{60}–OH or C_{60}–Por treatment (Fig. 6A). The total fluorescence intensity of individual cells was then analyzed, and the statistical results showed that both C_{60}–OH and C_{60}–Por treatments significantly reduced phagocytosis (Fig. 6B).

In view of the above results found that the surface ultrastructure and morphology have been restored to a certain extent, here we want to know whether the phagocytic function has been restored or not. THP-1 macrophages continued to be cultured in normal medium for 48 hours after C_{60}-fullerenes treatments, and then exposed to fluorescent beads overnight (Fig. 6A). The statistical results showed that the phagocytosis of both is increased noticeably (Fig. 6B). This is consistent with the

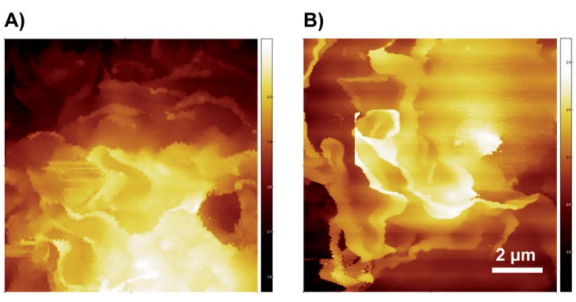

Fig. 4 Recoveries of the macrophage surface ultrastructure after different water-soluble C_{60}-fullerenes treatment. (A) Recovery after C_{60}–OH treatment. (B) Recovery after C_{60}–Por treatment. Region: 10 × 10 μm, pixel: 128 × 128.

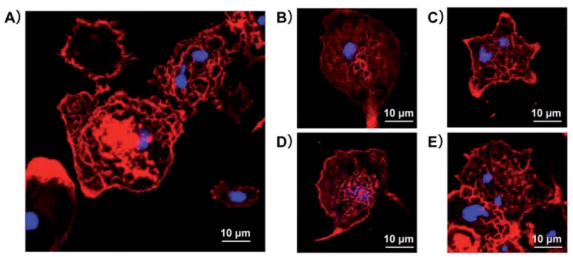

Fig. 5 Morphological changes of THP-1 macrophages after different water-soluble C_{60}-fullerenes treatment by using a confocal microscope. (A) Control. (B) Treat with C_{60}–OH. (C) Recovery after C_{60}–OH treatment. (D) Treat with C_{60}–Por. (E) Recovery after C_{60}–Por treatment. It is noted that the red actin was stained by rhodamine phalloidin, the cell nucleus was stained by DAPI.

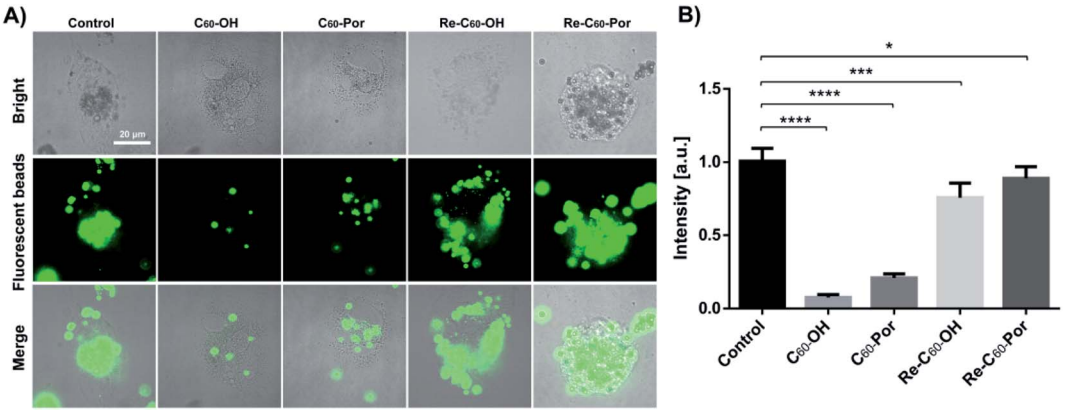

Fig. 6 The phagocytosis of THP-1 macrophage before and after treated with water-soluble fullerenes. (A) From left to right are the control, C_{60}–OH treatment, C_{60}–Por treatment, and recovery from C_{60}–OH and C_{60}–Por treatment respectively. The top row shows the bright field of THP-1 macrophages under different treatments. The middle row is the confocal images of 2 μm diameter fluorescent beads engulfed by macrophage. The bottom row is the overlap of bright fields and fluorescent fields. Scale bar, 20 μm. (B) The histograms show the corresponding average fluorescence intensity of about 30 cells each group.

previous results that the cellular morphology and surface ultrastructure cannot be fully restored. Therefore, we speculate that these two water-soluble fullerenes affect phagocytosis by affecting the rearrangement of surface membrane ruffles and intracellular actin cytoskeleton.

Conclusions

In conclusion, considering the wide application of fullerene derivatives in biomedicine, we hope to study their effects on the immune system by characterizing the relationship between the surface ultrastructure and function of immune cells. In this work, by using the contact-free SICM, we achieved the surface ultrastructure of macrophage under physiological conditions for the first time. Compared with the previous electron microscopy imaging results, we observed a lot of more intact sheet-like membrane ruffles. In addition, we found that the sheet-like surface membrane ruffles appeared varying degrees of shortening and thickening after treatment with C_{60}–OH or C_{60}–Por. And these changes could be restored basically when we removed the C_{60}-fullerenes derivatives and continued to culture in normal medium for 48 hours. Given that the membrane ruffles are shortened to varying degrees and the fluorescence intensity of F-actin on the membrane surface decreases after C_{60}–OH and C_{60}–Por treatment, we believe that the fullerenes induce cell membrane ruffle rearrangement by reducing F-actin aggregation or inhibiting F-actin protein expression. Further confocal imaging showed that most of the macrophage morphology turned round and the phagocytosis reduced significantly. Based on the negligible cytotoxicity of C_{60}–OH and C_{60}–Por, we could surmise that these two water-soluble C_{60}-fullerenes affected the phagocytosis of macrophage by affecting the surface membrane ruffles and intracellular actin cytoskeleton. And these effects were reversible to a certain degree.

Given the fact that membrane ruffles serve as a critical role in the initial capture of particulate targets prior to phagocytosis or micropinocytosis for activated macrophages, the membrane ruffle rearrangement is instrumental for the uptake of both soluble and particulate antigen by macrophages.[37,38] Therefore, C_{60}–OH and C_{60}–Por would be a promising inhibitor of phagocytosis in studying the endocytic mechanism. And this work also demonstrated that the contact-free SICM would be an excellent tool to study the morphological information of adhesive and fragile materials.

Conflicts of interest

There are no conflicts to declare.

Acknowledgements

This work was supported by the National Natural Science Foundation of China (21735006, 32000873, 22077124 and 91939301); the China Postdoctoral Science Foundation (2019M650718); the Chinese Academy of Sciences.

Notes and references

1 H. W. Kroto, J. R. Heath, S. C. O'Brien, R. F. Curl and R. E. Smalley, *Nature*, 1985, **318**, 162–163.
2 H. W. Kroto, A. Allaf and S. Balm, *Chem. Rev.*, 1991, **91**, 1213–1235.
3 D. M. Guldi and M. Prato, *Acc. Chem. Res.*, 2000, **33**, 695–703.
4 M. Mikawa, H. Kato, M. Okumura, M. Narazaki, Y. Kanazawa, N. Miwa and H. Shinohara, *Bioconjugate Chem.*, 2001, **12**, 510–514.
5 O. A. Kraevaya, A. V. Novikov, A. F. Shestakov, E. S. Ershova, E. A. Savinova, L. V. Kameneva, N. N. Veiko, D. Schols, J. Balzarini, S. V. Kostyuk and P. A. Troshin, *Chem. Commun.*, 2020, **56**, 10203–10206.
6 H. Ma, X. Zhang, Y. Yang, S. Li, J. Huo, Y. Liu, M. Guan, M. Zhen, C. Shu, J. Li and C. Wang, *Langmuir*, 2021, **37**, 2740–2748.
7 M. D. Esrafili and A. A. Khan, *RSC Adv.*, 2022, **12**, 3948–3956.

8 X. Zhang, W. Zhou, Y. Liu, L. Jin, J. Huo, Y. Yang, S. Li, H. Ma, J. Li, M. Zhen, J. Li and C. Wang, *Nano Res.*, 2022, **15**, 3346–3355.
9 C. M. Sayes, J. D. Fortner, W. Guo, D. Lyon, A. M. Boyd, K. D. Ausman, Y. J. Tao, B. Sitharaman, L. J. Wilson and J. B. Hughes, *Nano Lett.*, 2004, **4**, 1881–1887.
10 Y. Morimoto, M. Horie, N. Kobayashi, N. Shinohara and M. Shimada, *Acc. Chem. Res.*, 2012, **46**, 770–781.
11 S. Fiorito, A. Serafino, F. Andreola, A. Togna and G. Togna, *J. Nanosci. Nanotechnol.*, 2006, **6**, 591–599.
12 S. T. Stern and S. E. McNeil, *Toxicol. Sci.*, 2008, **101**, 4–21.
13 M. Lehto, T. Karilainen, T. Róg, O. Cramariuc, E. Vanhala, J. Tornaeus, H. Taberman, J. Jänis, H. Alenius and I. Vattulainen, *PLoS One*, 2014, **9**, e114490.
14 E.-J. Park, H. Kim, Y. Kim, J. Yi, K. Choi and K. Park, *Toxicol. Appl. Pharmacol.*, 2010, **244**, 226–233.
15 C. M. Sayes, A. M. Gobin, K. D. Ausman, J. Mendez, J. L. West and V. L. Colvin, *Biomaterials*, 2005, **26**, 7587–7595.
16 S. Yamago, H. Tokuyama, E. Nakamura, K. Kikuchi, S. Kananishi, K. Sueki, H. Nakahara, S. Enomoto and F. Ambe, *Chem. Biol.*, 1995, **2**, 385–389.
17 S. Fiorito, A. Serafino, F. Andreola and P. Bernier, *Carbon*, 2006, **44**, 1100–1105.
18 K. Ohsawa, Y. Imai, H. Kanazawa, Y. Sasaki and S. Kohsaka, *J. Cell Sci.*, 2000, **113**, 3073–3084.
19 M. Szabo, K. Dulka and K. Gulya, *Brain Res. Bull.*, 2016, **120**, 41–57.
20 M. Li, L. Liu, N. Xi, Y. Wang, X. Xiao and W. Zhang, *Langmuir*, 2014, **30**, 1609–1621.
21 A. Shvedova, V. Castranova, E. Kisin, D. Schwegler-Berry, A. Murray, V. Gandelsman, A. Maynard and P. Baron, *J. Toxicol. Environ. Health, Part A*, 2003, **66**, 1909–1926.
22 R. Tantra and A. Knight, *Nanotoxicology*, 2011, **5**, 381–392.
23 P. Hansma, B. Drake, O. Marti, S. Gould and C. Prater, *Science*, 1989, **243**, 641.
24 Y. E. Korchev, C. L. Bashford, M. Milovanovic, I. Vodyanoy and M. J. Lab, *Biophys. J.*, 1997, **73**, 653–658.
25 A. I. Shevchuk, G. I. Frolenkov, D. Sánchez, P. S. James, N. Freedman, M. J. Lab, R. Jones, D. Klenerman and Y. E. Korchev, *Angew. Chem.*, 2006, **118**, 2270–2274.
26 P. Novak, C. Li, A. I. Shevchuk, R. Stepanyan, M. Caldwell, S. Hughes, T. G. Smart, J. Gorelik, V. P. Ostanin and M. J. Lab, *Nat. Methods*, 2009, **6**, 279–281.
27 V. O. Nikolaev, A. Moshkov, A. R. Lyon, M. Miragoli, P. Novak, H. Paur, M. J. Lohse, Y. E. Korchev, S. E. Harding and J. Gorelik, *Science*, 2010, **327**, 1653–1657.
28 J. Seifert, J. Rheinlaender, P. Novak, Y. E. Korchev and T. E. Schäffer, *Langmuir*, 2015, **31**, 6807–6813.
29 P. Novak, A. Shevchuk, P. Ruenraroengsak, M. Miragoli, A. J. Thorley, D. Klenerman, M. J. Lab, T. D. Tetley, J. Gorelik and Y. E. Korchev, *Nano Lett.*, 2014, **14**, 1202–1207.
30 Y. Lee, G.-E. Jung, S. J. Cho, K. E. Geckeler and H. Fuchs, *Nanoscale*, 2013, **5**, 8577–8585.
31 J. A. Swanson, *Nat. Rev. Mol. Cell Biol.*, 2008, **9**, 639–649.
32 H. R. Petty, D. G. Hafeman and H. M. McCONNELL, *J. Cell Biol.*, 1981, **89**, 223–229.
33 T. Da Ros and M. Prato, *Chem. Commun.*, 1999, **8**, 663–669.
34 S. Ghrebi, D. W. Hamilton, J. Douglas Waterfield and D. M. Brunette, *J. Biomed. Mater. Res., Part A*, 2013, **101**, 2118–2128.
35 C. Zhou, Q. Liu, W. Xu, C. Wang and X. Fang, *Chem. Commun.*, 2011, **47**, 2982–2984.
36 S. Dang, Q. Liu, X. Zhang, K. He, C. Wang and X. Fang, *J. Nanosci. Nanotechnol.*, 2012, **12**, 4478–4484.
37 R. S. Flannagan, R. E. Harrison, C. M. Yip, K. Jaqaman and S. Grinstein, *J. Cell Biol.*, 2010, **191**, 1205–1218.
38 D. Schlam and J. Canton, *Small GTPases*, 2017, **8**, 65–70.